JOURNAL OF AIRCRAFT
Vol. 42, No. 1, January–February 2005

Parametric Studies of Transonic Aeroelastic Effects of an Aircraft Wing/Tip Store

Srinivasan Janardhan* and Ramana V. Grandhi†
Wright State University, Dayton, Ohio 45435
and
Frank Eastep‡ and Brian Sanders§
U.S. Air Force Research Laboratory, Wright–Patterson Air Force Base, Ohio 45433

This research investigates the effect of store parameters variation on store-induced flutter and limit-cycle oscillation phenomena of an aircraft wing in the transonic regime. The primary store parameters were its mass and the chordwise location of its center of gravity. The effect of including store aerodynamics on the wing/tip store configuration was also investigated. The tip store center of gravity (c.g.) was varied and positioned at three different locations: 32.5, 40, and 50%, with respect to aerodynamic tip chord. Automated Structural Optimization System and Computational Aeroelasticity Program–Transonic Small Disturbance were used in the linear and nonlinear region to perform this research. Studies showed that flutter speed increases as the store c.g. was moved forward toward the leading edge. This gives an indication that store c.g. must be placed as far forward as possible with respect to the elastic axis to delay the occurrence of flutter, while satisfying other design constraints. It was observed that the increase in tip store mass significantly reduced the flight operating speed range of the aircraft. The effect of inclusion of store aerodynamics for different wing/store configurations was found to be insignificant compared to their corresponding mass-only models in the transonic regime. The limit-cycle oscillation (LCO) onset speed was found to be sensitive to both store mass and store c.g. parameters and varied significantly for different store mass configurations. The LCO onset speed decreased significantly with increase in store mass and aft movement of store c.g.

Nomenclature

A	=	amplitude of a peak
C	=	generalized damping matrix
c_r	=	reference chord length
$f_0, \ldots f_3$	=	functions in transonic-small-disturbance equation defined by Eqs. (2–5)
G	=	splining matrix
g	=	damping ratio
h_i	=	ith splined mode shape obtained by the infinite plate spline technique
K	=	generalized stiffness matrix
k	=	reduced frequency, Hz
M	=	generalized mass matrix
n	=	number of peaks
Q	=	dynamic pressure, psf
q	=	generalized coordinates
S	=	wing area
t	=	nondimensional time
U	=	freestream velocity
x, y, z	=	Cartesian coordinates in the streamwise, spanwise, and vertical directions
x_i	=	ith structural mode shape
α	=	angle of attack, deg
γ	=	ratio of specific heats
ΔC_p	=	coefficient of lifting pressure
Δp	=	pressure difference between the lower and upper wing surface
δ_L	=	log decrement
ρ	=	freestream air density
ϕ	=	inviscid disturbance velocity potential

Received 30 January 2003; revision received 6 April 2004; accepted for publication 11 April 2004.

*Graduate Research Assistant, Department of Mechanical and Materials Engineering; sjanard@cs.wright.edu.
†Distinguished Professor, Department of Mechanical and Materials Engineering; rgrandhi@cs.wright.edu.
‡NRC Senior Research Associate; franklin.eastep@wpafb.af.mil.
§Senior Aerospace Engineer; Brian.Sanders@wpafb.af.mil.

Introduction

TODAY'S military aircraft can carry various configurations of external stores such as fuel tanks, missiles, bombs, and launchers. There are multiple positions available on the wing, where attachment of stores is possible, and one such position is at the wing tip. At the wing tip, again there are many combinations possible depending on the way store is attached. The presence and location of such external stores affect the structural, aerodynamic, and aeroelastic behavior of the wing. The mass or inertia parameters of the store also significantly affect the structural dynamic characteristics of the aircraft. Tip stores can change the aerodynamic and aeroelastic characteristics of a wing by the inertial, aerodynamic, and elastic coupling on the aircraft. The aeroelastic behavior of a tip store is very difficult to predict in the transonic region, as the governing equations in this region are highly nonlinear even under the assumption of small disturbance, which makes the flow process very complex. These nonlinearities arise primarily because of the geometry of the wing (such as the thickness, camber, and angle of attack) and the presence of strong moving shocks on the wing surface. The presence of stores, especially tip stores, can cause significant dynamic aeroelastic effects such as flutter and limit-cycle oscillation (LCO) in the transonic regime. They can lead to several problems in the target locking of an air-to-air missile attached at the wing tip and roll maneuverability of the entire aircraft. The occurrence of such unstable vibrations must be seriously considered and cleared off during the design of the wing structures. One of the main dynamic effects is LCO, which is generally encountered in external store configurations that are predicted to be flutter sensitive. LCO, though not catastrophic as compared to classical flutter, can lead to fatigue, which reduces the efficiency and structural reliability of the wing. The store-induced LCO is characterized by the

antisymmetric motion of the wing and stores and a lateral motion of the fuselage and aircrew. It has been described as a self-sustaining oscillation with constant amplitude that occurs as a result of nonlinear coupling between the dynamic response of the structure and the unsteady aerodynamic forces. LCO has also been described in the past as oscillations, in which the amplitude of motion is limited, cyclic, and oscillatory. Bunton and Denegri[1] have given a thorough description of LCO, its origin, and differences when compared to classical flutter.

Earlier research was concentrated mainly on the prediction of flutter point and LCO of an aircraft wing/tip store configuration in the supersonic and subsonic regime using models of varying accuracy. The linear flutter analysis methods predicted the flutter boundary reasonably accurately in the subsonic regime because of the negligible effects of compressibility and aerodynamic nonlinearities in this region. Very little work was done in the transonic region, which most of the fighter aircraft pass through, while accelerating from subsonic region to supersonic region. There were no reliable computational tools that could predict the unsteady aeroelastic phenomena such as flutter and LCO. Also, no work was performed in studying the sensitivity of flutter and LCO by changing the store parameters in the transonic region, as that would have facilitated in better understanding of such phenomena. This paper concentrates primarily on the sensitivity of flutter and LCO behavior to store structural parameters such as store c.g. location and mass in the transonic region; the effect of including store aerodynamics on flutter for different wing/store configurations; and prediction, onset, occurrence and severity of store-induced flutter and LCO in the transonic region. This study was performed to assist in the future store certification efforts, as a large number of flutter flight tests are carried out to certify the stores attached to different aircraft. This results in a huge amount of cost, time, and work force being used for each flight test. This research facilitates in gaining a better understanding of the behavior of flutter and LCO and developing a simulation-based design so as to reduce the number of flight tests to a few critical ones in the future store certification efforts.

The nonlinear aeroelastic analysis was performed using Computational Aeroelasticity Program–Transonic Small disturbance (CAP-TSD), which has proven in the past to be accurate while performing unsteady aeroelastic analysis. CAP-TSD, a computational-fluid-dynamics (CFD) code, is based on the transonic-small-Disturbance (TSD) theory. A wing structure was chosen on which flutter and LCO studies were conducted. Every effort was made to model the wing to possess real fighter aircraft wing characteristics. The finite element model was used to represent stiffness and mass properties of the wing and store. Vibration modes were used by CAP-TSD during the aeroelastic analysis to model the structure and were obtained from Automated Structural Optimization System (ASTROS)[2] modal analysis. Flutter analysis was carried out in both subsonic and transonic regimes using ASTROS and CAP-TSD to demonstrate the need for nonlinear aerodynamic analysis. However, LCO was found to occur mainly in the transonic region as a result of the addition of stores at various locations. Linear flutter analysis identified the frequency of oscillation and modal mechanism of LCO. However, because of the lack of effect of the nonlinearities, the linear flutter analysis failed to predict the onset or severity of LCO, which are extremely important during store certification efforts.

Previous Literature

In the past, Denegri[3] has investigated the response of an oscillatory wing during flutter flight tests of several external store configurations in the transonic region. He found that the response could be divided into various categories representing a broad range of aeroelastic responses encountered by a fighter aircraft with external stores. The influence of a tip store on transonic aeroelastic stability has been examined by Guruswamy et al.[4] He conducted flutter analysis for rectangular- and fighter-type wings with tip stores using ATRAN3S code in the transonic region. It was shown that the tip store could make the wing aeroelastically unstable. However, no studies were conducted to investigate any variation of flutter or LCO behavior with store parameters. In the 1980s, Triplett[5] conducted linear flutter analysis on an F/A-18 wing carrying a tip store using the doublet-lattice method in the subsonic regime, but he did not analyze in the transonic region.

Turner[6] performed an analytical study on the effect of store aerodynamics using MSC/NASTRAN on a large number of wing/store configurations to develop general guidelines. However, it was possible only to generate specific guidelines for the inclusion of store aerodynamics for a particular aircraft. In another case, Striz and Jang[7] approximated the tip missile without fin geometry in the aerodynamic model and conducted their flutter analysis. Kim and Lee[8] performed aeroelastic analyses in the transonic and supersonic flow regions using a computational-fluid-dynamics technique (TSD3KR) for computing the unsteady aerodynamics in conjunction with MSC/NASTRAN for the flutter analysis of a wing with a tip store. They conducted a matched-point flutter analysis to obtain the flutter solutions in both the frequency and time domain. They showed that the effect of tip store could change the flutter stability of the wing structure significantly.

Jun et al.[9] have studied the influence of a wing-tip missile on the multidisciplinary design optimization of a wing structure subjected to design constraints using ASTROS*.[10] Their studies indicated that the store aerodynamics must be included during the aft positioning of tip missile. All of these studies were conducted for the subsonic and supersonic regions. The flutter behavior was found to be very sensitive to the tip missile position along the tip chord. Pitt and Fuglsang[11] have performed static and dynamic aeroelastic calculations on F-15 and F/A-18 wings using CAP-TSD. They have indicated the need for inclusion of nonlinear aerodynamics for both static and dynamic aeroelastic calculations in the transonic region, when compared with the corresponding linear analysis results. They effectively used CAP-TSD to demonstrate its capabilities to calculate aerodynamic effects, such as flutter and aileron reversal speed, using TSD theory. However, no sensitivity studies with respect to store parameters on the variation in flutter and LCO were presented in their research.

As compared to the flutter phenomena, the LCO occurs only with wing/store combinations and predominantly in the transonic flow regions. The LCO phenomenon is a complex flow process, and recent renewed interest has further motivated to understand the flow physics of such flow process. A lot of literature is available investigating the occurrence and behavior of LCO using both experimental and computational techniques. Many researchers such as Kim and Strganac[12] analyzed LCO of an aircraft wing by considering structural, aerodynamic, and store-induced nonlinearities together. Recently, Beran et al.[13] has conducted CAP-TSD and ENS3DAE analyses on a Goland wing to determine the range of applicability of the various mathematical models in predicting the store-induced LCO. Chen et al.[14] assumed that nonlinear structural damping was a significant factor in the rise of a specific type of LCO, which occurred mainly in a low subsonic Mach-number region. He conducted analysis on two aircraft configurations that differed only in the missile launcher positions: one underwing and the other on the wing tip. The results showed a "humped" damping curve with stability transitions, which correlated to the onset and subsequent stopping of the LCO, measured during flight tests. Cunningham and Meijer[15] believed that the wing/store LCO was largely caused by the transonic shock oscillations and shock-induced flow separation, called transonic shock/separation (TSS) model. Thomas et al.[16] developed a LCO solution technique to obtain the LCO response based on unsteady aerodynamics provided by a frequency-domain harmonic balance method for the nonlinear inviscid CFD model. This study was conducted on a transonic airfoil configuration. With this technique, both stable and unstable LCO responses were computed efficiently. Tang et al.[17] investigated the effects of viscosity, including turbulence modeling and TSS, among other mechanisms, on the transonic LCO. He found that the viscous effects play an important role in the accurate prediction of shock and LCO. Also, a small initial perturbation produces large-amplitude LCO at small mean pitch angle and plunge, while a large initial perturbation appears to produce small or negligible amplitude LCO at larger mean values.

Bendiksen and Kousen[18,19] studied the nonlinear effects on transonic flutter using an explicit time-accurate Euler code. With their Euler model coupled with the solution of a two-degrees-of-freedom airfoil structural model, they showed the possibility of LCO in a transonic flow.

Transonic Small-Disturbance Theory

CAP-TSD, developed by Batina et al.,[20] utilizes the TSD theory to solve unsteady aeroelastic problems in realistic aircraft configurations. The advantage of using TSD formulation is the relatively low computational cost, the simplicity of the gridding and geometry preprocessing, and the ability to treat complete aircraft configuration. The code uses a time-accurate approximate-factorization (AF) algorithm for an efficient solution of unsteady TSD equation. The AF algorithm consists of a time-linearization procedure coupled with an internal subiteration technique. For unsteady flow calculations, the solution procedure involves two steps. First, a time-linearization step is performed to determine an estimate of the potential field. Second, subiterations are performed to minimize the linearization and factorization errors. CAP-TSD is capable of treating combinations of lifting surfaces and bodies. In the TSD theory, the flow is assumed to be governed by a general frequency modified TSD potential equation written in conservation law form as

$$\frac{\partial f_0}{\partial t} + \frac{\partial f_1}{\partial x} + \frac{\partial f_2}{\partial y} + \frac{\partial f_3}{\partial z} = 0 \tag{1}$$

where

$$f_0 = -A\phi_t - B\phi_x \tag{2}$$

$$f_1 = E\phi_x + F\phi_x^2 + G\phi_y^2 \tag{3}$$

$$f_2 = \phi_y + H\phi_x\phi_y \tag{4}$$

$$f_3 = \phi_z \tag{5}$$

The coefficients A, B, and E are defined as

$$A = M_\infty^2, \qquad B = 2M_\infty^2, \qquad E = 1 - M_\infty^2 \tag{6}$$

where M_∞ is the far-field Mach number.

F, G, and H depend on the assumptions used in deriving the TSD equation. For nonlinear analysis, the coefficients are

$$F = -\tfrac{1}{2}(\gamma + 1)M_\infty^2, \qquad G = -\tfrac{1}{2}(\gamma - 3)M_\infty^2$$

$$H = -(\gamma - 1)M_\infty^2 \tag{7}$$

and for linear analysis,

$$F = 0, \qquad G = 0, \qquad H = 0 \tag{8}$$

In the preceding equations, γ is the ratio of specific heat at constant pressure to specific heat at constant volume (1.4 for air). For steady flow calculations, after time linearization, internal subiterations are not used because time accuracy is not necessary when marching toward steady state. The solution of TSD equation is the converged steady-state velocity potentials from which aerodynamic pressures are calculated. The aeroelastic computational procedure implemented within CAP-TSD includes the simultaneous integration of structural equations of motion and unsteady aerodynamic time-marching solution procedure.

An inviscid version of CAP-TSD code was used for this research. This is because even though inclusion of viscous effects produces more accurate results they are computationally intensive and expensive compared to the inviscid version. Moreover, for flows involving weak or moderately strong embedded shock waves inviscid computations using the TSD equations have produced accurate solutions for thin airfoils,[21] thin wings,[22] wing-canard combinations,[23] and realistic aircraft configurations.[24] As shock waves increase in strength and move aft on the airfoil, viscous effects become significant and must be accounted for in the calculations to obtain accurate solutions.[25] For attached flows, integral boundary-layer methods can be coupled with the inviscid analysis by viscous-inviscid iteration. These interactive boundary-layer techniques have produced viscous solutions that agree well with experimental results.[26]

The viscous-inviscid interaction version of CAP-TSD code[27] interactively couples the inviscid TSD algorithm with an inverse integral boundary-layer model and has been used effectively to compute the viscous flow effects involving mildly separated and separation onset flows.[28] The boundary-layer equations are solved in a quasi-steady formulation similar to that recommended by Green et al.[29] The three-dimensional viscous effects are incorporated into the CAP-TSD code in a stripwise manner. In viscous CAP-TSD code, the outer inviscid solution and the inner viscous solution are computed independently and are coupled using an active control mechanism that minimizes the coupling errors for unsteady flows.

Research Approach

The aeroelastic equations of motion for an elastic wing can be formulated in terms of generalized coordinates of modal motion $q(t)$, which is a solution to the following equation:

$$M\ddot{q} + C\dot{q} + Kq = \boldsymbol{Q}(t) \tag{9}$$

$Q(t)$ is the vector of generalized aerodynamic forces that is discretized into Q_i by the splining technique. Q_i is the generalized aerodynamic force associated with q_i, which is computed by integrating the pressure distribution on the wing surface as

$$Q_i = \rho\frac{U^2c_r^2}{2}\int_s h_i\frac{\Delta p}{\rho U^2/2}\frac{\mathrm{d}S}{c_r^2}, \qquad \Delta C_p = \frac{\Delta p}{\rho U^2/2} \tag{10}$$

and h_i is obtained as

$$h_i = [G]x_i \tag{11}$$

where $[G]$ is the splining matrix, which interpolates the structural modes onto the aerodynamic grid.

Equation (11) implies two steps: 1) modal reduction of equations of motion and 2) spline interpolation of forces and displacements from structural grid to aerodynamic grid and vice versa. The equation of motion (9) for the free-vibration case can be rewritten as

$$\ddot{q} = -M^{-1}Kq - M^{-1}C\dot{q} \tag{12}$$

In the case of structural dynamic analysis, the preceding governing equation was solved (ignoring the aerodynamic forces term). This equation was solved using ASTROS to obtain the natural frequencies, mode shapes, generalized mass, and stiffness, which will be used by CAP-TSD to model the structure. The aeroelastic equations of motion in CAP-TSD are based on a right-hand orthogonal coordinate system with the x direction defined as positive downstream and the z direction positive upward.

Before the aeroelastic analysis was performed, the convergence of the CAP-TSD wing grid lines resolution was examined through steady-state aerodynamic calculations. Examining the wing steady pressure helps to assess the basic character of the flowfield. The unsteady flowfield, and hence generalized aerodynamic forces, depend strongly on the steady-state flow, especially in the transonic speed range. Thus, the steady pressure distributions frequently can give mechanisms that control the aeroelastic phenomena.

Static aeroelastic analysis was performed using a value of dynamic pressure that is assumed to be near the velocity that produces flutter (neutral stability). For this, many simulation runs were executed. Static aeroelastic analysis yields a steady-state flowfield, thus providing the starting flowfield for the dynamic aeroelastic analysis.

The dynamic aeroelastic analysis was initiated by restarting from the converged static aeroelastic solution. A small initial disturbance was given on the vertical velocity of the wing,

$$\dot{x}_0 = 1.0 \text{ in./s} \tag{13}$$

From the preceding analysis, generalized displacements of each mode at each time step were obtained. Unsteady pressure distribution was also obtained from this analysis.

The coefficient of lift obtained from different instants of time was plotted. The damping ratio value was computed as

$$\delta_L = (1/n)\,\ell_n(A_n/A_0), \qquad g = \delta_L \Big/ \sqrt{4\pi^2 + \delta_L^2} \tag{14}$$

where A_n is the amplitude of nth peak in C_L vs time-steps plot and A_0 is the amplitude of first peak in C_L vs time-steps plot.

When the damping ratio value moves from a negative damping to a positive damping direction and crosses the zero damping, the flutter speed is obtained.

Wing-Structure Model

In the initial phase, the wing structure used in Refs. 30 and 31 was considered. The present study required modifications in the preceding wing structure. In the previous studies, the semispan for the structural model of the wing was 90 in., while the aerodynamic model span was 108 in. To attach the tip store aerodynamic model to the wing model, the structural semispan was extended to the same length as the aerodynamic model. The structural model was extended by 20% of its original length so as to be completely superimposed by the aerodynamic model. The three spars were simply extended in their original directions for the required length.

The wing structure[32] was a two-cell wing box. Figure 1 illustrates the finite element model of the wing structure. It had a root chord of 48 in. and a tip chord of 26.5 in. The semispan was extended from 90 to 108 in. It was modeled using 120 finite elements, out of which 48 plate bending elements were used to represent the wing skins, 42 shear panels represented the spars and ribs, and 30 rod elements represented the posts and were used to connect the upper and lower skin nodes. The material used was aluminum ($E = 10.3 \times 10^6$ psi).

The wing root was built by fully constraining all of the structural nodes at the root. No other constraints were applied at other nodes and all had six degrees of freedom. The nonstructural weight added at various structural nodes represented the weight of the structure outside (at the leading and trailing edges) and was attached to the wing and consisted of other miscellaneous weights, such as fuel, control system, etc. The nonstructural weights were distributed in such a way that each internal node carried 6 lb, while each boundary node carried 9 lb. The total nonstructural weight was 378 lb. There were no nonstructural weights at the tip of the wing, as store was attached at those points. The structural weight of the wing was 90.7 lb. The rod cross-sectional area was set to 0.1 in.^{2} The center of gravity was located at 46.14% of the root chord. The elastic axis was located at 44% of the root chord. The ratio of nonstructural weight to structural weight was 4.16.

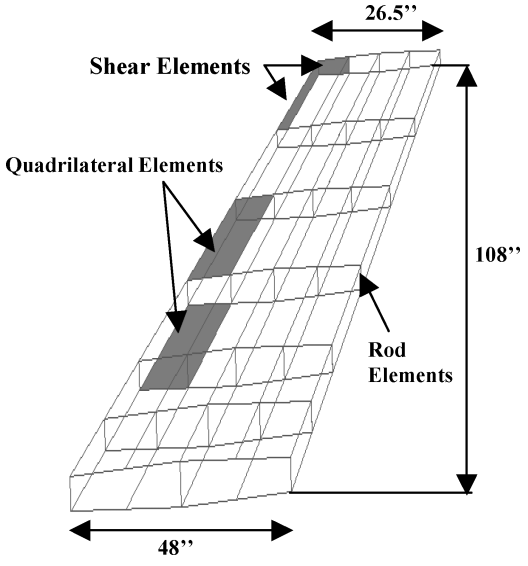

Fig. 1 Wing-structure finite element model.

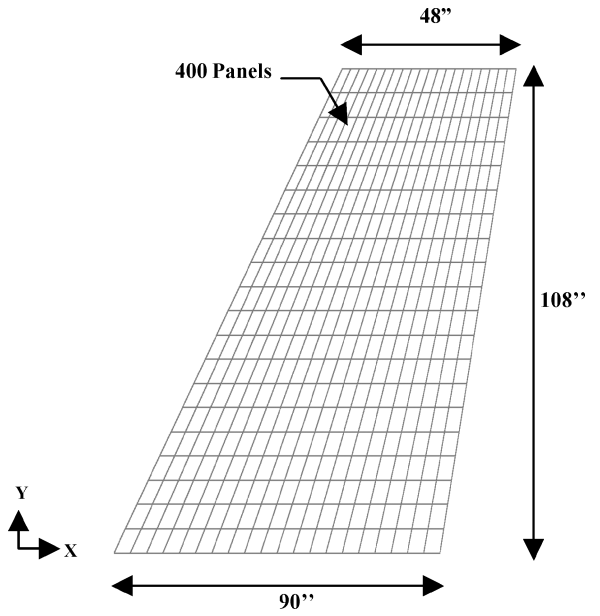

Fig. 2 Doublet-lattice method/ASTROS aerodynamic model of wing.

Wing Aerodynamic Model

An aerodynamic model, as shown in Fig. 2, was developed to provide unsteady aerodynamics for the ASTROS flutter analysis. The aerodynamic model for the wing planform was defined by 400 panels using doublet-lattice aerodynamics. There were 20 spanwise and 20 chordwise panels in the model. The spanwise and chordwise panels were equally spaced. The root chord and tip chord were 90 and 48 in., respectively. The wing semispan was 108 in. The wing had an aspect ratio of 2.33. The aerodynamic parameters were calculated at aerodynamic grids, which do not generally coincide with the structural grid points. Therefore, splining technique was used to transfer the structural displacements and aerodynamic forces from one set of grids to the other.

In case of CAP-TSD, the wing was also modeled both in the physical and computational domain. The physical region boundary of the wing was defined in a similar manner as the ASTROS aerodynamic model. All of the dimensions in CAP-TSD modeling were normalized using the reference chord length (in this case, aerodynamic root chord). The CAP-TSD computational grid for the wing chosen had 90 streamwise gridlines (with 50 gridlines per wing chord), 30 spanwise gridlines (with 20 gridlines on the wing), and 60 vertical grid lines. A thin airfoil shape was chosen for all of the aeroelastic analyses in the linear and nonlinear region. Figure 3 shows the NACA 4% thick, symmetrical airfoil with zero camber and angle of attack.

Store Description

The store was attached to the wing at the tip. Figure 4 shows the structural model of the store connected to the wing at 50% of the aerodynamic tip chord. The store structural model was represented using BAR elements with seven grid points. The length of each element was uniformly distributed throughout the store. A model of six elements was developed to represent the store. The store was approximated without any fins and had a length of 79.5 in. The structural weight of the store was 154.1 lb, and the nonstructural weight added was 77 lb. The nonstructural weight represented the guidance and control system, etc. The store body was made of steel (modulus of elasticity: $E = 30 \times 10^6$ psi; specific weight $= 0.33$ lb/in.^{3}). The area moments of inertia were $I_1 = I_2 = 14.86$ in.^{4} and torsion constant, $J = 29.72$ in.^{4} The wing was joined to the store using BAR elements. It was assumed that the attachments were rigid. The stiffness of material used as attachments was very high compared to the stiffness of store. The attachments were configured in a V shape. Each end of the connection element was attached to the top skin and bottom skin nodes of the wing tip.

Fig. 3 NACA 4% thick airfoil.

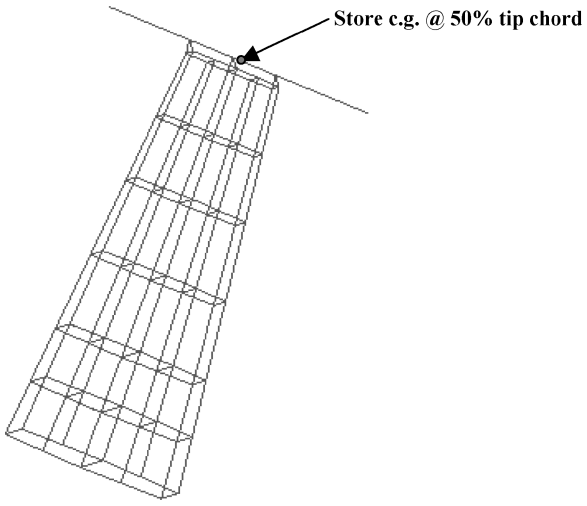

Fig. 4 Finite element model of wing with tip store c.g. at 50% tip chord.

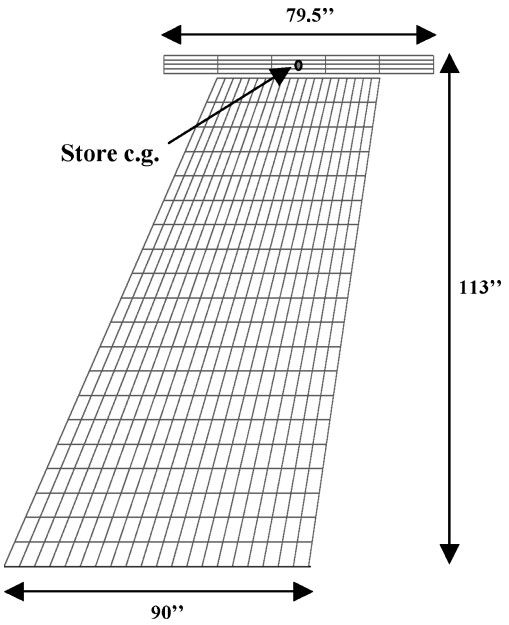

Fig. 5 Doublet-lattice method/ASTROS aerodynamic model of wing with tip store c.g. at 50% tip chord.

Figure 5 shows the aerodynamic model of store attached to the wing at 50% aerodynamic tip chord. The model was generated using the ASTROS aerodynamic modeling scheme. The store was modeled as flat panels using doublet-lattice aerodynamics. The store model was generated using 25 panels and was divided in both chordwise and spanwise directions into five equal divisions each.

Results from ASTROS and Discussion

The natural frequencies and vibration mode shapes represent the dynamic characteristics of the wing model. Vibration analysis was performed on the clean wing and different wing/tip store configurations using ASTROS. The mode shapes for a clean wing and a wing with tip store c.g. at 50% tip chord (mass only) are shown in Figs. 6 and 7. There was a switching of modes from bending to fore-aft mode when the store was attached. The combination of a bending and torsional mode in the case of a clean wing changed to a fore-aft mode because of store attachment. For a clean wing, the fourth mode was a fore-aft mode. This mode does not contribute anything to the dynamic characteristics and flutter behavior of the wing. The magnitude of frequency separation of the first and second modes for a clean wing was large compared to the separation between the third and the fourth modes. The vibration frequencies for a wing with the tip store c.g. at 50% tip chord (mass-only) reduced by more than 50% when compared to the clean wing results. This was due to the inertia effect of the store attached to the wing. The mode shapes for 32.5 and 40% configuration were similar to the 50% configuration.

The flutter analysis was conducted for both subsonic and transonic Mach numbers in ASTROS. P-K method was used for the flutter speed calculations. A sea-level density ratio was maintained throughout the calculations. Velocity-damping (V-g) diagram was used to locate the flutter point by computing the speed corresponding to zero damping value. In flutter analysis, the effect of store modeling on the wing was considered in two ways. In the first case, the store was considered a mass-only model. This means that the aerodynamics of the store was not included. The store contributed only inertia and structural characteristics. In the second case, aerodynamics of the store was also included along with the mass.

Figure 8 shows the V-g diagram for comparison of a clean wing and a wing/store configuration at 50% tip chord (both with and without store aerodynamics). The figure represents the effect of including the store aerodynamics on flutter speed. The analysis was conducted using ASTROS at a transonic Mach number of 0.9. However, one needs to remember that ASTROS treats the transonic Mach numbers linearly. Therefore, the flutter speeds computed for transonic Mach numbers will have inaccuracies because of the lack of nonlinearities. The first mode was the mode of instability showing a similar pattern of failure for both the mass-only model and the model with store aerodynamics. The flutter speed for the wing/tip store c.g. at 50% tip chord (mass only) was found to be 545.025 knots, whereas the flutter speed for the same configuration with store aerodynamics included was 455.208 kn. There was a 16.48% decrease in flutter speed in the case of a wing/store configuration with store aerodynamics, when compared with the corresponding wing/store mass-only model. The severity of flutter was determined from the fact that the wing/store model with store aerodynamics was rapidly becoming unstable, and the slope of instability curve was very steep compared to the wing/store mass-only model.

The flutter sensitivity to store c.g. location with respect to the wing aerodynamic tip chord was analyzed using different wing/store cases. The store was positioned in the same manner as the wing/tip store c.g. at 50% tip chord. To obtain the required configurations, the store was maintained at the same position, but the c.g. was moved to locate an exact position of 32.5, 40, and 50% with respect to the wing aerodynamic tip chord by redistributing the non-structural weight of the store.

The V-g plot showing flutter characteristics of the wing/store (mass-only) models at different store c.g. locations is shown in Fig. 9. The pattern of failure was pretty much the same as the wing/store configuration with store aerodynamics, but the amplitude of damping was less for the mass-only model cases compared to the corresponding cases where the store aerodynamics was included. The results indicated that the tendency of the tip store to undergo flutter was less when it was attached closer to the leading edge when compared to other configurations.

Figure 10 shows a V-g diagram representing the sensitivity of flutter to different store c.g. locations (including store aerodynamics). As the store c.g. was moved aft of the elastic axis of the wing, the flutter speed decreased rapidly. In all three wing/store configurations, the first mode was the mode of instability. The slope of

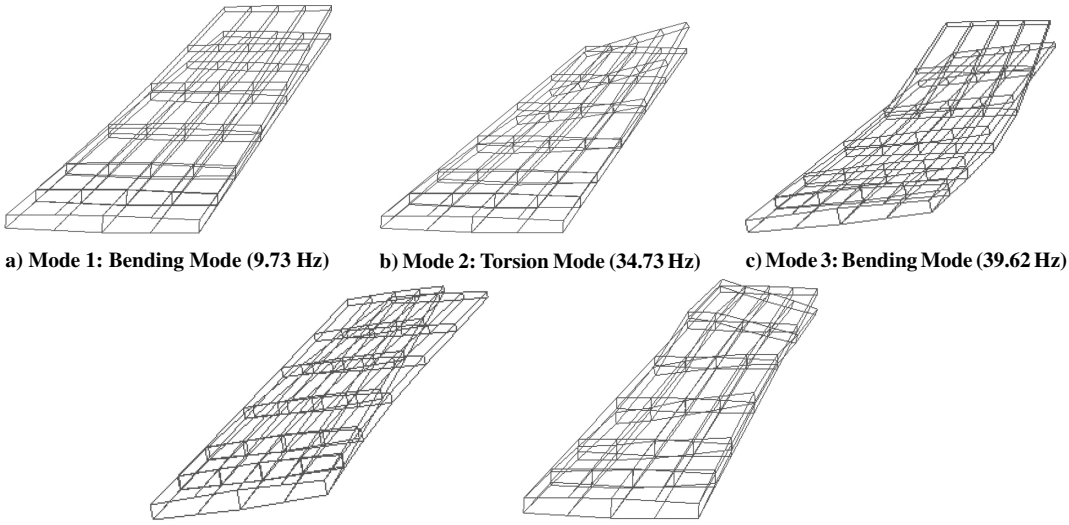

a) Mode 1: Bending Mode (9.73 Hz) b) Mode 2: Torsion Mode (34.73 Hz) c) Mode 3: Bending Mode (39.62 Hz)

d) Mode 4: Fore-aft Mode (45.60 Hz) e) Mode 5: Bending/Torsion Mode (69.61 Hz)

Fig. 6 Mode shapes of clean wing.

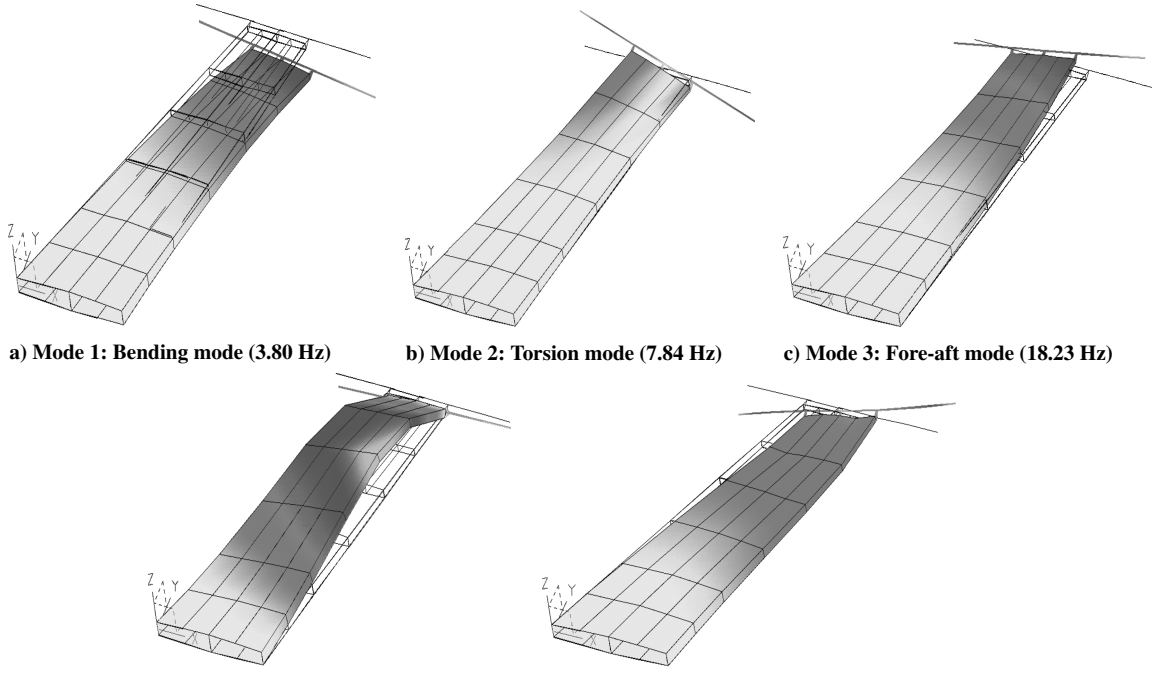

a) Mode 1: Bending mode (3.80 Hz) b) Mode 2: Torsion mode (7.84 Hz) c) Mode 3: Fore-aft mode (18.23 Hz)

d) Mode 4: Bending mode (20.39 Hz) e) Mode 5: Fore-aft mode (46.99 Hz)

Fig. 7 Mode shapes of wing with store c.g. at 50% tip chord.

instability became very steep when store c.g. was at 50% tip chord compared to other wing/store configurations and the clean wing. The flutter mode crossed the zero damping line locating the flutter point. However, the flutter mode crossed the zero damping line again after sometime, thus forming a hump mode. This gives an indication of the region in which LCO might occur, though linear flutter analysis failed to predict the onset or severity of LCO accurately because of a lack of nonlinearities involved. As the store c.g. was moved aft of the elastic axis, the hump mode characteristics started to slowly disappear, and the flutter characteristics started becoming dominant. This gives an indication that moving the store c.g. forward of the elastic axis would delay the occurrence of flutter.

Results from CAP-TSD and Discussion

To accurately predict the flutter speed and LCO onset speed in the transonic region by including the aerodynamic nonlinearities, an inviscid version of CAP-TSD was used. Aeroelastic analysis in CAP-TSD was carried out in generalized modal coordinates. The wing was modeled both in physical and computational regions. The aeroelastic analysis was performed for different values of velocity and dynamic pressure, assuming a constant sea-level density (unmatched flutter analysis). Structural damping was assumed to be zero for all cases. The angle of attack of the wing was taken as zero, and a $90 \times 30 \times 60$ grid was used to calculate the unsteady parameters for all of the cases. Grid points were clustered along the edges and normal to the wing and store geometry. The grid was generated externally by calculating grid-point distributions for all three of the coordinate directions. In CAP-TSD, the lifting surfaces were modeled as thin plates. The upper- and lower-surface data of each horizontal lifting surface were supplied to provide the thickness and camber information. The wing was modeled structurally using the first six modes while still retaining the characteristics of the basic flutter mechanism. These vibration modes were obtained

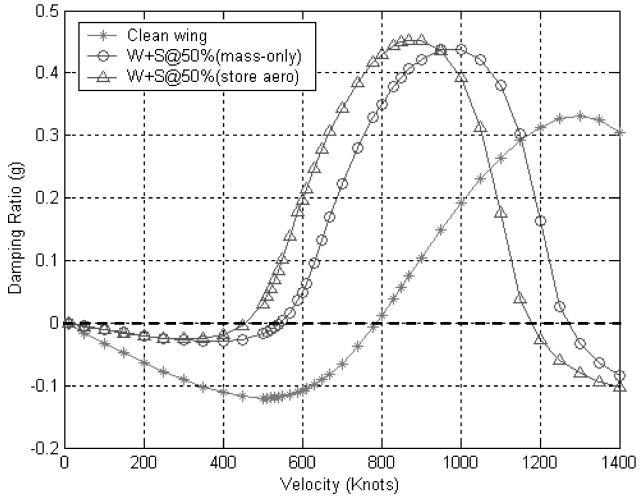

Fig. 8 V-g plot showing the effect of including store aerodynamics on flutter (Mach 0.9, sea-level, doublet-lattice method/ASTROS).

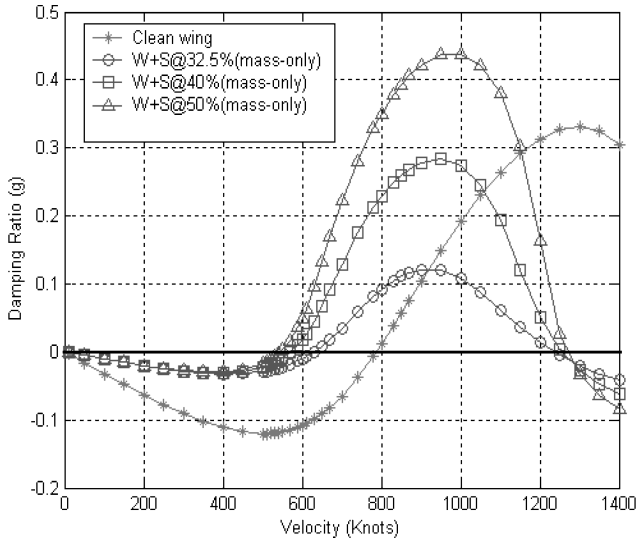

Fig. 9 V-g plot for sensitivity of flutter to store c.g. location using different wing/store (mass-only) models (Mach 0.9, sea-level, doublet-lattice method/ASTROS).

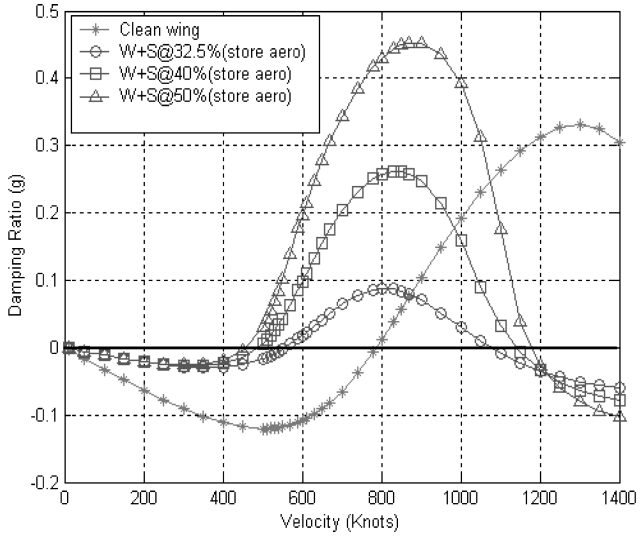

Fig. 10 V-g plot for sensitivity of flutter to store c.g. location using different wing/store (store aero) models (Mach 0.9, sea-level, doublet-lattice method/ASTROS).

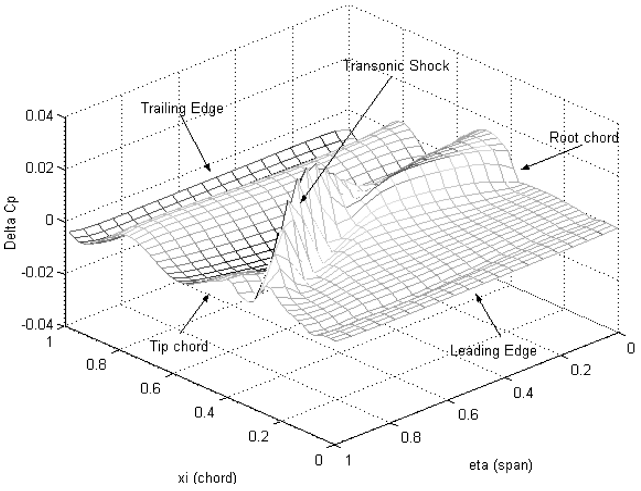

Fig. 11 Unsteady pressure distribution for a clean wing at $V = 669$ kn, Mach 0.9.

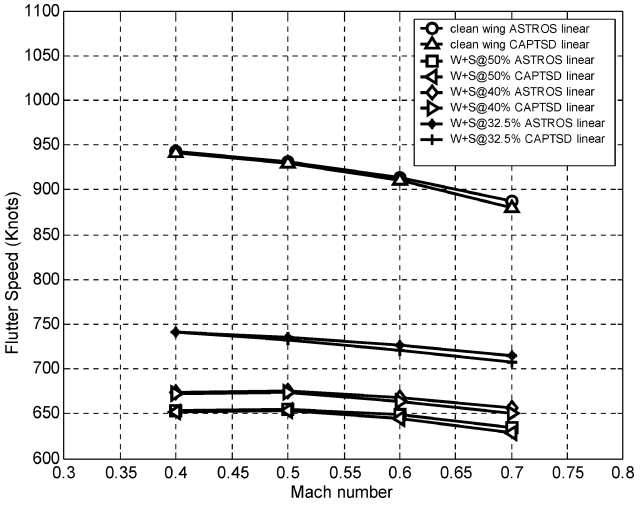

Fig. 12 Comparison of linear flutter analysis for different store c.g. configurations.

from ASTROS modal analysis. The structural displacements were splined onto the aerodynamic grid of CAP-TSD.

The CAP-TSD dynamic aeroelastic analysis was performed in two stages. In the first stage, a static aeroelastic analysis was performed using nonlinear CAP-TSD aerodynamics. Static aeroelastic analysis resulted in a steady-state flowfield to account for wing thickness, camber, and mean angle of attack, thus providing the starting flowfield for the dynamic aeroelastic analysis. In the second stage, the dynamic aeroelastic analysis was initiated from the converged static solution by providing a small disturbance to each of the modal velocities to begin the structural integration. The disturbance in velocities for each mode was provided rather than displacements, as it helps in avoiding nonphysical, strictly numerical transients and their possible instabilities. Figure 11 shows the unsteady pressure distribution for a clean wing at Mach 0.9 for a velocity $V = 669$ kn on the computational grid. Transonic shock waves traveled from the root chord to the tip chord. These shocks drastically change the pressure distribution on the surface of the wing, thereby affecting the occurrence of flutter and LCO. This poses problems in correctly predicting the flutter speed for the given flow conditions. These shocks appear because of the nonlinear effects of mixed flow in the transonic region. The flutter speed was calculated by interpolating the various damping values to locate the speed corresponding to zero damping.

Figure 12 shows the comparison of flutter speeds obtained using doublet-lattice aerodynamics and transonic small-disturbance

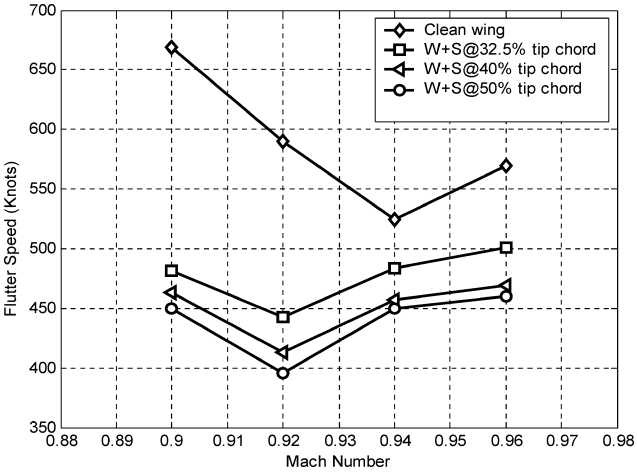

Fig. 13 Sensitivity of flutter speed to store c.g. location for transonic Mach numbers (mass-only models).

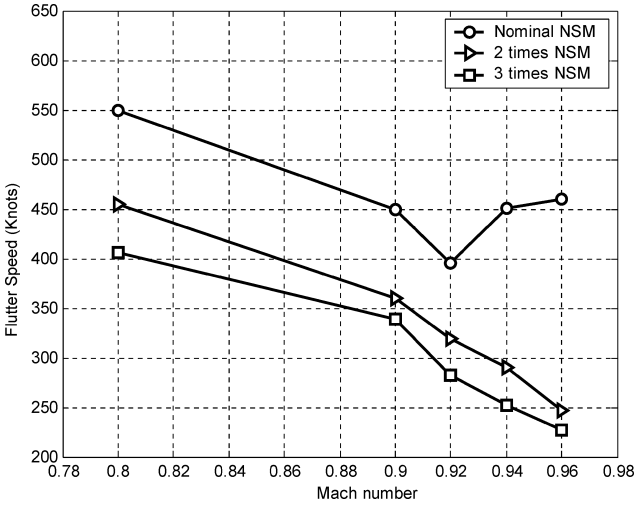

Fig. 14 Sensitivity of flutter speed to store mass for different tip store mass configurations in the transonic regime.

theory in the linear subsonic region. The flutter speeds obtained using the two theories matched well at low Mach numbers. This was done to check for consistency in the linear region before moving onto the nonlinear region. Flutter boundaries were computed for clean wing and other wing/store configurations. For a clean wing, CAP-TSD predicted a flutter speed of 883 kn at Mach 0.7, a value 0.5% lower than that predicted by ASTROS. For the wing/store configuration at 50% tip chord, CAP-TSD predicted a flutter speed of 631 kn, a value 0.54% lower than that predicted by ASTROS. Similarly, CAP-TSD and ASTROS linear flutter analysis were conducted for the wing/store configurations at three store c.g. locations and compared. The flutter results were found to match well, and as the Mach number increased the difference in flutter velocities increased because of the minor effects of nonlinearities in the high subsonic region.

Sensitivity in the behavior of flutter in the clean wing and the three wing/store (mass-only) configurations at different c.g. locations for different transonic Mach numbers is shown in Fig. 13. The behavior was studied to examine the range of applicability of computed flutter speeds of an aircraft carrying tip store in the nonlinear region. It also indicates the sensitivity of flutter to different store c.g. locations in the transonic region. The figure represents a flutter boundary for different Mach numbers that divides the region into a stable and unstable section. In this case, the inertia properties and aerodynamics of the wing alone were considered, whereas only the inertia characteristics of the store were included. The wing and store structures were represented in the form of vibration modes. A transonic dip was observed at Mach 0.94 for the clean wing, with a flutter speed of 525 kn, whereas transonic dip occurred at Mach 0.92 for the three wing/store configurations, thereby effectively reducing the flight envelope of the aircraft. The dip was characterized by a sudden drop in flutter speed before rising again at high transonic Mach numbers. It was observed that moving the store c.g. forward of the elastic axis shifted the transonic dip to a higher flutter speed at the same Mach number. The flutter boundary was very sensitive to the Mach number for all of the configurations near the transonic dip region. The occurrence of transonic dip was caused by the presence of shock waves that increased in strength and moved as the Mach number increased.

Figure 14 represents the sensitivity of flutter speed to store inertia parameter, namely, the tip store mass. In this analysis, only the wing with tip store c.g. at 50% configuration was chosen because this represented the extreme case of flutter as shown in the preceding case. No store aerodynamics was included, as the effect of inclusion of store aerodynamics on flutter speed was found to be negligible for such wing/tip store configurations. In the first case, the initial nonstructural mass (NSM) was used, and then the store NSM was assigned twice the initial store NSM, and in the third case it was made three times. It was earlier found that a transonic dip occurred at Mach 0.92 when the initial store mass was attached, but no such behavior was observed when the store mass was increased. The disappearance of transonic dip for heavier store configurations could be related to the coupled aeroelastic nonlinearities involved in the transonic flow process. In fact, as the nonstructural store mass was doubled or tripled, the flutter speed kept decreasing with the Mach number even beyond Mach 0.92. This indicates that increasing the store mass could lead to a decrease in the range of flight speeds in which a fighter aircraft can operate. As the store mass was increased, the percentage difference in flutter speed between any two successive configurations decreased. There was a steep drop in flutter speed after Mach 0.9.

The impact of including the store aerodynamics while modeling the store in the transonic region was also studied. This study was carried out to facilitate in deciding whether store aerodynamics need to be included while performing multidisciplinary design optimization of the wing structure to delay the occurrence of store-induced flutter and LCO in the transonic region. The optimization algorithms are highly iterative in nature and computationally intensive; therefore, including the store aerodynamic model could make the whole procedure even more time-consuming and difficult. Therefore, flutter speeds of store c.g. and store mass configurations (both mass-only and including store aerodynamics) were computed both in the subsonic and transonic region. The flutter results of different store c.g. and store mass configurations (both mass-only and including store aerodynamics) matched well in the linear subsonic region. However, in order to understand the impact of including the store aerodynamics in the nonlinear region, the flutter results of store c.g. and store mass configurations (both mass-only and including store aerodynamics) are represented in Figs. 15 and 16, respectively, for Mach 0.8–0.96. Figure 15 shows that there was not much difference in the flutter speeds between the store mass-only models and when the store aerodynamics was also included for the different wing/tip store c.g. configurations. However, addition of store aerodynamics had a positive effect on all of the three wing/tip store c.g. configurations beyond Mach 0.92. But the overall percentage difference remained almost the same for all of the configurations. In Fig. 16, the flutter speeds as a result of store aerodynamics for the three store mass configurations did not vary significantly when compared to their corresponding mass-only cases. The overall percentage difference was in the range of approximately 0–7%, based on all of the cases in the transonic regime. This range of difference in flutter speeds matched well with the results reported by Turner.[6] For some cases, the flutter speed computed for store aerodynamics matched almost exactly with their corresponding mass-only cases. The flutter speed for wing/tip store at 50% mass-only configuration was 450 kn, whereas for the corresponding store aerodynamics case was 425.67 kn at a Mach 0.9. The percentage difference was

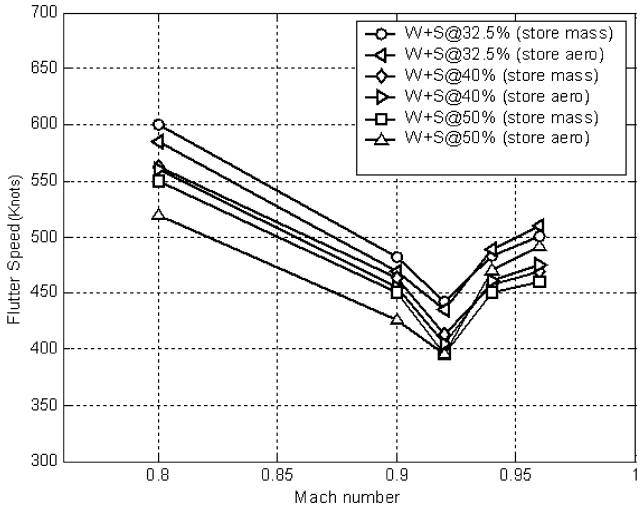

Fig. 15 Effect of inclusion of store aerodynamics for different tip store c.g. in the transonic regime.

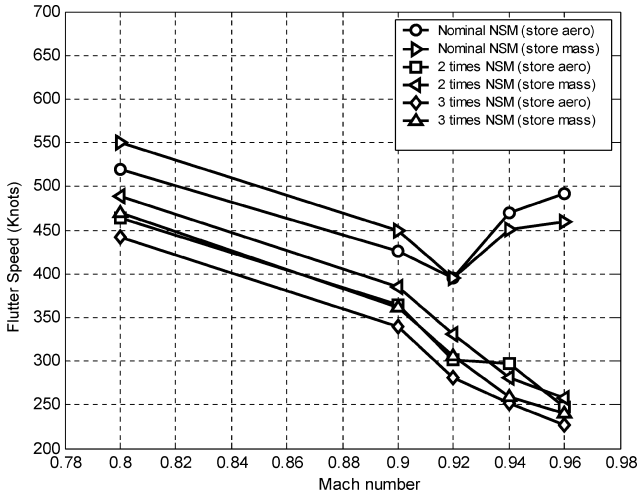

Fig. 16 Effect of inclusion of store aerodynamics for different tip store mass in the transonic regime.

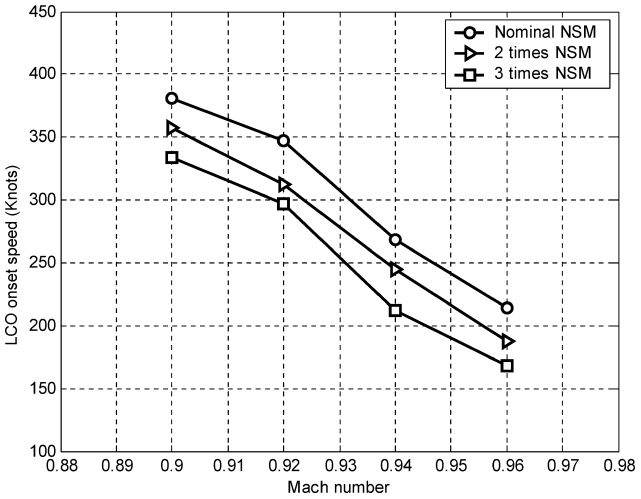

Fig. 17 Sensitivity of LCO onset speed to store mass for transonic Mach numbers.

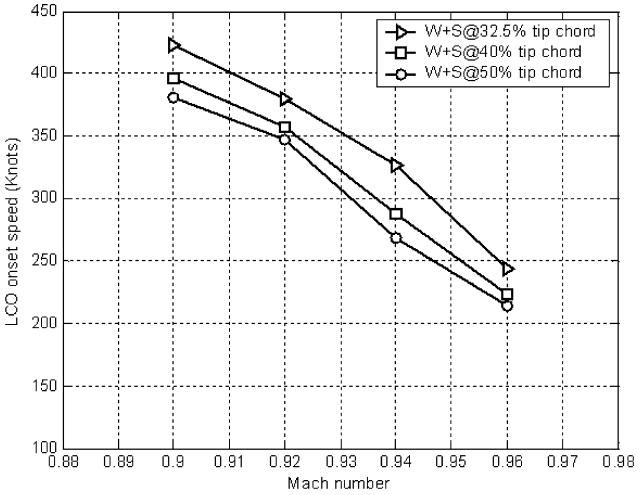

Fig. 18 Sensitivity of LCO onset speed to tip store c.g. in the transonic regime.

approximately 5.4%. For the same case, the linear theory failed to correctly predict the flutter speed in the transonic regime. Actually, the impact of including store aerodynamics on the flutter speed depends on the problem, and in this case the inclusion of store aerodynamics, although modeling the store, did not have any significant effect when compared to the corresponding mass-only model. Another interesting thing observed was that in the case of wing/store configuration at 50% aerodynamic tip chord, the flutter speed, when the store aerodynamics was included, was more than the corresponding mass-only configuration for higher transonic Mach numbers (Mach 0.94, 0.96), compared to lower transonic Mach numbers (Mach 0.8, 0.9, 0.92).

Figure 17 shows the sensitivity of LCO onset speed to store mass computed for a range of transonic Mach numbers for the three wing/tip store configurations using CAP-TSD. LCO was observed to occur mainly in a restricted Mach-number range. In the case of a clean wing, no LCO was found to occur in the transonic region. For all of the wing/store configurations, LCO occurred only after Mach 0.9. No LCO was observed in the linear region and the initial transonic region. This is because LCO is a highly nonlinear phenomenon, due to which the linear aerodynamic theories are unable to capture its occurrence. The LCO onset speed was computed for each wing/store configuration in the high transonic Mach-number range (Mach 0.9–0.96). The LCO onset speed was found to decrease rapidly as the store mass was increased. For a given Mach 0.94, the LCO onset speed reduced by approximately 13%, as the store nonstructural mass was first doubled and then tripled. The slope of the LCO curve for each configuration was approximately the same. Severity of LCO over a transonic Mach-number range can be observed in the steep slope of the curve for each configuration, indicating that the addition of store mass for a given configuration might create a greater tendency to undergo LCO in the transonic regime.

Figure 18 shows the sensitivity of LCO onset speed to location of the store center of gravity. The nonlinear aeroelastic analysis was performed on three different wing/tip store configurations with store c.g. at 32.5, 40, and 50% tip chord (mass only). LCO onset speed was found to be sensitive to the store c.g. locations. For a small change in store c.g. location, the LCO onset speed for a given Mach number, changed by a large number. At Mach 0.94, as the store c.g. position varied by 7.5%, the LCO onset speed changed by approximately 20%. It can be observed from the figure that as the store c.g. position was moved aft the percentage decrease in LCO onset speed reduced for successive store c.g. locations. However, the slope and hence the severity of occurrence of LCO was almost the same for all of the three wing/tip store configurations. As the Mach number increased, the LCO onset speed decreased rapidly. This was because at higher Mach-number values the aerodynamic flow became increasingly nonlinear, and the shock effects over the entire region became predominant.

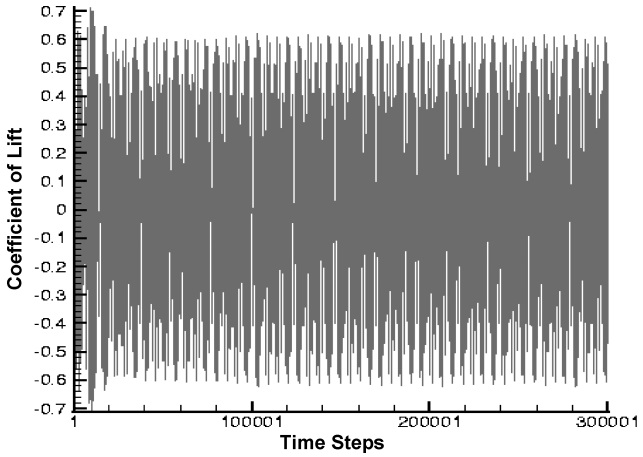

Fig. 19 Wing with tip store c.g. @50% (mass-only) showing LCO at 380 kn at Mach 0.9.

Figure 19 shows LCO response occurring at a speed of 380 kn for the wing with tip store c.g. at 50% tip chord (mass-only) configuration at Mach 0.9. The amplitude of the LCO was found to be quite large, representative of the characteristics of the nonlinear phenomena in the transonic region. The amplitude of LCO increases with the increase in speed, and at one point it becomes so large that the transonic small-disturbance theory assumptions become invalid under such conditions. This large amplitude of LCO response can be reduced in magnitude by including the viscous effects into the modeling of transonic flows. The computed LCO solution had an oscillation frequency of 4.21 Hz. The LCO response consisted of contributions mainly from first bending and torsion modes. The frequency value was very close to the first bending mode of 3.80 Hz of the preceding wing/tip store configuration that represented the dominant participation of the first modal response in the occurrence of LCO phenomena. However, there was also a strong participation from the second mode. The two modes were more strongly coupled to each other than the flutter modes. From the frequency values obtained, the LCO frequency lied in between the first bending mode and the flutter frequency with more inclination towards the first bending mode. A similar mechanism was found in other cases also. The LCO mechanism was similar to the flutter mechanism, as the bending mode was the dominant instability mode in both cases. In all of the LCO computations, the store was not modeled aerodynamically, as it was shown by Beran et al.,[13] so that the inclusion of store aerodynamics did not have any significant impact on the LCO computations for the inviscid flow cases when compared to their corresponding store mass configurations using CAP-TSD. Moreover, the onset speed of LCO is computationally intensive to obtain as very large integration time is necessary for the aeroelastic system to approach time-asymptotic behavior at values of flight speed near critical.

Conclusions

This research was intended to analyze the effect of varying the store parameters on different wing/store configurations in the transonic region and provide more information to enable in future store certification efforts. The store structural parameters investigated were location of store c.g. with respect to the aerodynamic tip chord and store mass. The effect of including store aerodynamics was also investigated for different wing/store configurations in the transonic regime.

Linear aeroelastic analysis results using ASTROS for clean wing and different wing/store c.g. configurations matched well with the CAP-TSD linear analysis results for their corresponding configurations. This was done to check for consistency in the linear region before entering the nonlinear (transonic) region.

Comparisons of flutter results for the clean wing and wing/store configurations for different store c.g. locations using ASTROS were presented. Flutter results were also presented for clean wing and a particular (store c.g. at 50% tip chord) wing/store configuration (mass-only model) using CAP-TSD. In both cases, it was found that moving the store c.g. forward relative to the elastic axis had a stabilizing effect by increasing the flutter speed. Therefore, the store should be attached as far forward as possible, simultaneously satisfying other design constraints so as to delay the occurrence of flutter.

Addition of store aerodynamics decreased the flutter speed of the wing/store configuration by 16.48% as compared to the store mass-only model, when doublet-lattice aerodynamic theory was used for flutter prediction. However, the TSD theory did not indicate much difference in flutter results between the mass-only model and the store aerodynamics model. Overall, the difference in flutter speeds for the two types of configurations was found to be in the range of 0–7% in the nonlinear region that matched well with the results reported in a previous paper.

Transonic dip was found to occur at an earlier Mach number in the wing/store configurations compared to the clean wing. This could effectively reduce the flight envelope of the aircraft and thereby inhibit the accomplishments of the mission critical tasks. Sensitivity of flutter speed to the store mass was also analyzed, and it was found that increasing the store mass reduced the flutter speed significantly. Transonic dip was found to occur for an initial store mass for the given configuration, but as the store mass was increased the behavior disappeared. For higher Mach numbers and store mass values, the flutter speed was found to decrease rapidly. No occurrence of LCO was found in the clean wing configuration throughout the transonic Mach number range. Store-induced LCO onset speed was found to be very sensitive to the store mass and store c.g. location in the transonic regime. The LCO onset speed decreased rapidly in the highly nonlinear region with increase in store mass and aft movement of store center of gravity position. This LCO behavior with respect to the transonic Mach numbers could pose several problems in flying an aircraft in the operating speed range.

Acknowledgments

This research work was sponsored by the Air Force Office of Scientific Research under the Grant F49620-01-1-0179. The authors acknowledge the support of Narendra S. Khot and Phil Beran of Wright-Patterson Air Force Base, Ohio, for their valuable suggestions and John Edwards and David M. Schuster of NASA Langley Research Center, Hampton, Virginia, for providing the Computational Aeroelasticity Program–Transonic-Small-Disturbance code.

References

[1]Bunton, R. W., and Denegri, C. M., Jr., "Limit Cycle Oscillation Characteristics of Fighter Aircraft," *Journal of Aircraft*, Vol. 37, No. 5, 2000, pp. 916–918.

[2]Johnson, E., and Venkayya, V. B., "Automated Structural Optimization System (ASTROS)," Vol. I Theoretical Manual, U.S. Air Force Wright Aeronautical Labs., TR-88-3028, Dayton, OH, Dec. 1988.

[3]Denegri, C. M., Jr., "Limit Cycle Oscillations Flight Test Results of a Fighter with External Stores," *Proceedings of 41st AIAA/ASME/ASCE/AHS/ASC Structures, Structural Dynamics and Material Conference and Exhibit*, Atlanta, GA, 3–6 April 2000; also AIAA Paper 2000-1394, April 2000.

[4]Guruswamy, G. P., Goorjian, P. M., and Tu, E. L., "Transonic Aeroelasticity of Wings with Tip Stores," *Proceedings of 27th Structures, Structural Dynamics and Materials Conference*, San Antonio, TX, 19–21 May 1986, pp. 672–682; also AIAA Paper 1986-1007, May 1986.

[5]Triplett, W. E., "Wind Tunnel Correlation Study of Aerodynamic Modeling for F/A-18 Wing-Store Tip-Missile Flutter," *Journal of Aircraft*, Vol. 21, No. 8, 1984, pp. 329–334.

[6]Turner, C., "Effect of Store Aerodynamics on Wing/Store Flutter," *Journal of Aircraft*, Vol. 19, No. 7, 1982, pp. 574–580.

[7]Striz, A. G., and Jang, S. K., "Optimization of Wing Tip Store Modeling," *Journal of Aircraft*, Vol. 24, No. 8, 1987, pp. 516–517.

[8]Kim, D., and Lee, I., "Transonic and Supersonic Flutter Characteristics of a Wing-Box Model with Tip Stores," *Proceedings of 42nd AIAA/ASME/ASCE/AHS/ASC Structures, Structural Dynamics, and Material Conference and Exhibit*, Seattle, WA, 16–19 April 2001; also AIAA Paper 2001-1464, April 2001.

[9]Jun, S., Tischler, V. A., and Venkayya, V. B., "Multidisciplinary Design Optimization of a Built-up Wing Structure with Tip Missile," *Proceedings of 43rd AIAA/ASME/ASCE/AHS/ASC Structures, Structural Dynamics and Materials Conference and Exhibit*, Denver, CO, 22–25 April 2002; also AIAA Paper 2002-1421, April 2002.

[10]Chen, P., Sarhaddi, D., and Liu, D., "Development of the Aerodynamic/Aeroservoelastic Modules in ASTROS," *ZAERO Programmer's Manual*, Vol. 2, U.S. Air Force Research Lab., AFRL-VA-WP-TR-1999-3050, Wright–Patterson AFB, OH, Feb. 1999.

[11]Pitt, D. M., and Fuglsang, D. F., "Aeroelastic Calculations for Fighter Aircraft Using the Transonic Small Disturbance Equation," *Transonic Unsteady Aerodynamics and Aeroelasticity*, Paper No. 16, AGARD-CP-507, March 1992, pp. 16-1–16-11.

[12]Kim, K., and Strganac, T. W., "Aeroelastic Studies of a Cantilever Wing with Structural and Aerodynamic Nonlinearities," *Proceedings of 43rd AIAA/ASME/ASCE/AHS/ASC Structures, Structural Dynamics and Materials Conference and Exhibit*, Denver, CO, 22–25 April 2002; also AIAA Paper 2002-1412, April 2002.

[13]Beran, P. S., Khot, N. S., Eastep, F. E., Snyder, R. D., Zweber, J. V., Huttsell, L. J., and Scott, J. N., "The Dependence of Store-Induced Limit-Cycle Oscillation Predictions on Modelling Fidelity," *Proceedings of the RTO Applied Vehicle Technology Panel Symposium on Reduction of Military Vehicle Acquisition Time and Cost Through Advanced Modeling and Virtual Product Simulation*, Paris, France, 22–25 April 2002, Paper 44.

[14]Chen, P. C., Sarhaddi, D., and Liu, D. D., "Limit-Cycle Oscillation Studies of a Fighter with External Stores," *Proceedings of 39th AIAA/ASME/ASCE/AHS/ASC Structures, Structural Dynamics and Material Conference and Exhibit*, Long Beach, CA, 20–23 April, 1998; also AIAA Paper 1998-1727.

[15]Cunningham, A. M., Jr., and Meijer, J. J., "Semi-Empirical Unsteady Aerodynamics for Modeling Aircraft Limit-Cycle Oscillations and Other Nonlinear Aeroelastic Problems," *International Forum on Aeroelasticity and Structural Dynamics*, ICAS/Royal Aeronautical Society, Manchester, U.K., June 1995.

[16]Thomas, J. P., Dowell, E., and Hall, K., "Nonlinear Inviscid Aerodynamic Effects on Transonic Divergence, Flutter and Limit-Cycle Oscillations," *AIAA Journal*, Vol. 40, No. 4, 2002, pp. 638–646.

[17]Tang, L., Bartels, R. E., Chen, P. C., and Liu, D. D., "Simulation of Limit Cycle Oscillations Using a CFD Time-Marching Method," *Proceedings of 42nd AIAA/ASME/ASCE/AHS/ASC Structures, Structural Dynamics, and Materials Conference and Exhibit*, Seattle, WA, 16–19 April 2001; also AIAA Paper 2001-1290.

[18]Bendiksen, O. O., and Kousen, K. A., "Transonic Flutter Analysis Using the Euler Equation," *Proceedings of AIAA Dynamics Specialist Conference*, Monterey, CA, 9–10 April 1987; also AIAA Paper 1987-0911.

[19]Kousen, K. A., and Bendiksen, O. O., "Limit Cycle Phenomena in Computational Transonic Aeroelasticity," *Journal of Aircraft*, Vol. 31, No. 6, 1994, pp. 1257–1263.

[20]Batina, J. T., Seidal, D. A., Bland, S. R., and Bennett, R. M., "Unsteady Transonic Flow Calculations for Realistic Aircraft Configurations," *Journal of Aircraft*, Vol. 26, No. 1, 1989, pp. 21–28.

[21]Batina, J. T., "Unsteady Transonic Algorithm Improvements for Realistic Aircraft Applications," *Journal of Aircraft*, Vol. 26, No. 2, 1989, pp. 131–139.

[22]Bland, S. R., and Seidel, D. A., "Calculation of Unsteady Aerodynamics for Four AGARD Standard Aeroelastic Configurations," NASA TM-85817, 1984.

[23]Bennett, R. M., and Batina, J. T., "Application of the CAP-TSD Unsteady Transonic Small Disturbance Program to Wing Flutter," *Proceedings-European Forum on Aeroelasticity and Structural Dynamics*, DGLR-Bericht 89-01, Deutsche Gesellschaft fur Luft- und Raumfahrt e.V., 1989, pp. 25–34.

[24]Batina, J. T., "Unsteady Transonic Flow Calculations for Interfering Lifting Surface Configurations," *Journal of Aircraft*, Vol. 23, No. 5, 1986, pp. 422–430.

[25]Melnik, R. E., Chow, R. R., Mead, H. R., and Jameson, A., "An Improved Viscid/Inviscid Interaction Procedure for Transonic Flow over Airfoils," NASA CR-3805, 1985.

[26]Howlett, J., "Calculation of Unsteady Transonic Flows with Mild Separation by Viscous-Inviscid Interaction," NASA TP-3197, June 1992.

[27]Edwards, J. W., "Transonic Shock Oscillations Calculated with a New Interactive Boundary Layer Coupling Method," AIAA Paper 93-0777, Jan. 1993.

[28]Edwards, J. W., "Calculated Viscous and Scale Effects on Transonic Aeroelasticity," *Numerical Unsteady Aerodynamic and Aeroelastic Simulation*, AGARD-R-822, AGARD, Neuilly-sur-Seine, France, March 1998, pp. 1-1–1-11.

[29]Green, J. E., Weeks, D. J., and Brooman, J. W. F., "Prediction of Turbulent Boundary Layers and Wakes in Compressible Flow by a Lag-Entrainment Method," British Aeronautical Research Council, R&M No. 3791, London, 1977.

[30]Wilkinson, K., Lerner, E., and Taylor, R. F., "Practical Design of Minimum-Weight Aircraft Structures for Strength and Flutter Requirements," *Journal of Aircraft*, Vol. 13, No. 18, 1976, pp. 614–624.

[31]Hemmig, F. G., Venkayya, V. B., and Eastep, F. E., "Flutter Speed Degradation of Damaged, Optimized Flight Vehicles," *Journal of Aircraft*, Vol. 17, No. 12, 1980, pp. 833, 834.

[32]Janardhan, S., Grandhi, R. V., Eastep, F. E., and Sanders, B., "Design Studies of Transonic Flutter and Limit-Cycle Oscillation of an Aircraft Wing/Tip Store," *Proceedings of 44th AIAA/ASME/ASCE/ AHS Structures, Structural Dynamics and Materials Conference and Exhibit*, Norfolk, VA, 17–20 April 2003; also AIAA Paper 2003-1944.